

PIV in a model wind turbine rotor wake

Knud Erik Meyer¹, Igor V. Naumov², Ivan Kabardin², Robert Mikkelsen³ and Jens Nørkær Sørensen³

¹ Department of Mechanical Engineering, Technical University of Denmark, Denmark, kem@mek.dtu.dk

² Institute of Thermophysics, SB RAS, Novosibirsk, Russia

³ Department of Wind Energy, Technical University of Denmark, Denmark

ABSTRACT

Stereoscopic particle image velocimetry (PIV) measurements of the flow in the wake of scale model of a horizontal axis wind turbine is presented. Near the rotor, measurements are made in vertical planes intersecting the rotor axis. These planes capture flow effect from the tip and root vortices. The stability of the tip vortices as a function of different tip speed ratios are demonstrated. An instability seems to occur after a time corresponding to four blade passages. The result is vortex pairing and in some cases grouping of three vortices. Further downstream in the wake, measurements in planes perpendicular to the rotor axis is used to investigate the dynamics in the far wake. Here, a precessing core is found and data indicate that the Strouhal number of the precessing is independent of the rotor speed.

1. Introduction

The wake from a wind turbine rotor consists of a low speed region, a series of helical tip vortices and a series of root vortices. Our experiment aims both to investigate if the rotor works as designed and to investigate the dynamics of the wake. The latter is of great importance in wind farms where a wind turbine often is placed in the wake of another wind turbine. The wake dynamics will influence the power production since the recovery rate of the wake will influence the wind speed seen by downstream turbines. A just as important problem is that the wake contains small and large flow structures that downstream turbines will see as increased turbulence. This increases the fatigue load on the turbine and impacts the design requirement, maintenance and in the end the Cost of Energy (CoE).

Wind turbine wakes are difficult to study in full scale both because of the size of the turbines and because the incoming flow cannot be controlled and is difficult to document in detail simultaneously with measurements in the wake. Full scale measurements of the detailed wake behaviour and development has been reported using LiDAR [1], however, with limited part of the wake being captured as data are retrieved within a conical area downstream seen from the turbine hub. Experiments have therefore mostly been pursued at model scale. Particle image velocimetry (PIV) is becoming a popular technique for this purpose because significant flow structures can be captured. An early example of PIV measurements on wind turbine models is reported by Whale *et al* [2]. Measurements on a larger model (rotor diameter 4.5 m) in the European MEXICO program is reported by Schepers and Snel [3]. The large model is an advantage in terms of higher Reynolds number, but it also results in relatively smaller fields of view for PIV. In the last few years, the number of studies involving PIV has increased significantly. An example is the study by Sherry *et al* [4]. They investigate the tip and root vortices for a model in a water flume. This study and most other studies uses two-component PIV. The study by Zhang *et al* [5] is one of the very few that uses stereoscopic PIV.

Many studies use quite simple rotor blades. An example is [5] that uses nearly flat plates as blades. Such blades will easily experience stall on the blades and this can influence the dynamics in the wake flow and the formation of tip vortices. The present study combines elements from [4] and [5]. A scale model wind turbine rotor is designed using airfoils and design principles used on full size wind turbines. The experiments are carried out in a water flume to achieve higher Reynolds numbers, and stereoscopic PIV is used to provide additional information about the flow. The present paper is a first report on the measurements. Further measurements and more thorough data analysis are planned for future publication.

2. Experimental set-up

We have designed an experiment with a small three-blade horizontal axis wind turbine rotor placed in a water flume. The water flume has a length of 35 m, a width of 3 m and a water height of 0.9 m. The inlet to the flume consists of a contraction and a “honeycomb” flow straightener. The measurements are performed 20 m downstream of the inlet. Here, the boundary layer thickness is about 0.1 m. The rotor is placed in the part that has uniform velocity. The turbulence intensity was found to be less than 3%.

The rotor diameter is $D = 2R = 0.376$ m and the blades have a length of 0.159 m. The blades uses the SD7003 blade profile [6] and the chord and angle of attack along span were calculated by the Glauert’s theory for an optimal windmill [7] with the tip speed ratio $\lambda = \Omega R/U = 5$. Here, Ω is the angular speed of the rotor and U is the free stream velocity. The rotor blades is design to operate at an expected Reynolds number of 20 000-80 000 which suggest that sectional profile drag is high, $C_{L,max}$ and maximum C_L/C_D low. Based on this a design lift coefficient of $C_L = 0.8$ at $Re = 60\,000$ was chosen for the rotor blades. The rotor is mounted on a $0.4D$ long axis,

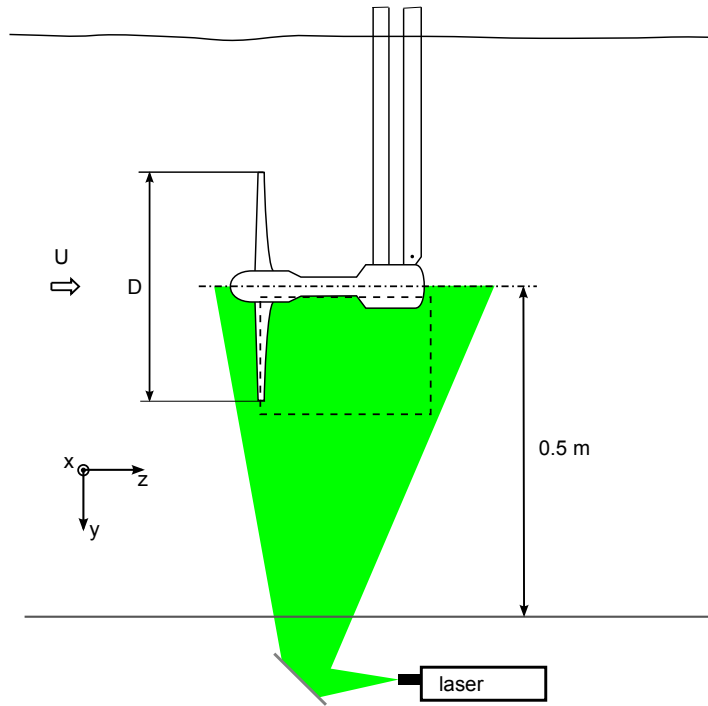


Figure 1: Sketch of experimental setup. A typical field of view is marked with dashed line.

see figure 1. The axis consists of the rotor hub with a diameter of 54 mm and then a part with a diameter of 32 mm. The axis is mounted in a cylindrical gearbox with diameter of about 70 mm. The gearbox contains an encoder and rotor speed control. It is hold by two cylinders (first is circular, second is square) and is carried by a movable platform above the water surface. The encoder can be used to trigger PIV recordings at specific rotor angles θ . The Reynolds number based on tip speed and blade chord is typically $Re = 20000$. The coordinate system used has origin at the center of the rotor hub (where rotor axis and blade axes intersect). The z coordinate follows the rotor axis in downstream direction, x is horizontal direction and y goes vertically downwards. Velocity components in the x , y and z direction are denoted u , v and w .

Stereoscopic Particle Image Velocimetry (PIV) are done in vertical planes aligned with the rotor axis (see figure 1) or planes in the rotor wake perpendicular to the rotor axis. The laser sheet created by a 200 mJ Nd:YAG laser enters the setup through a window in the bottom of the flume. Two CCD cameras (Dantec Hisense, 1280×1024 pixels) have optical access through water-filled prisms mounted at windows in each of the side walls downstream of the rotor. The cameras have 60 mm focal length lenses hold by Scheimpflug mounts. The optical axis of the lenses are horizontal with an angle of approximately 45° with the rotor axis. The measurement region typically has a size of $0.7D \times 0.5D$. The PIV system is moved relatively to the rotor to several positions to cover a large part of the wake and also upstream conditions. The data series near the rotor cover several rotor positions (rotor angle θ) in steps of 15° . Finally, several tip speed ratios λ are investigated.

Calibration of the stereoscopic setup is done with a planar target with a dotted pattern. The target is moved to five different positions in the out-of-plane direction. The calibration is based on a third order polynomial.

3. Visualization

Figure 2 shows visualization made by dye sources placed on the blades near the tip and near the root. The rotor axis is here mounted on a slender box different from the gear box is used in the PIV measurements. Tip vortices are clearly indicated showing a nearly perfect helical shape. Further downstream, instabilities create irregularities in this vortex pattern. Helical root vortices are also seen near the rotor axis.

4. Wake near rotor

The wake flow near the rotor is investigated using planes aligned with the rotor axis as illustrated in figure 1. By traversing the rotor, the measurement plane is moved in the y and z directions. The free stream velocity is $U = 0.38$ m/s. For each tip speed ratio λ and rotor angle θ , 100 snapshots are taken. The images are processed with LaVision Davis version 8.1.4 using 32×32 pixel interrogation windows. An example of a measurement is shown in figure 3a that shows the phase-average of the 100 snapshots taken for $\lambda = 5$ and $\theta = 45^\circ$. In the region of $y/D \approx 0.1$ and $z/D < 0.2$, some artifacts are caused by the presence of the rotor hub and reflections from one of the blades. In the region of $y/D \approx 0.1$ and $z/D > 0.5$, the gearbox extends into the image causing reflections and hence wrong vectors. Narrow regions at the top and bottom in the right side of the plot have exactly zero velocity and this denotes regions with no data due no overlap between the images from the two cameras.

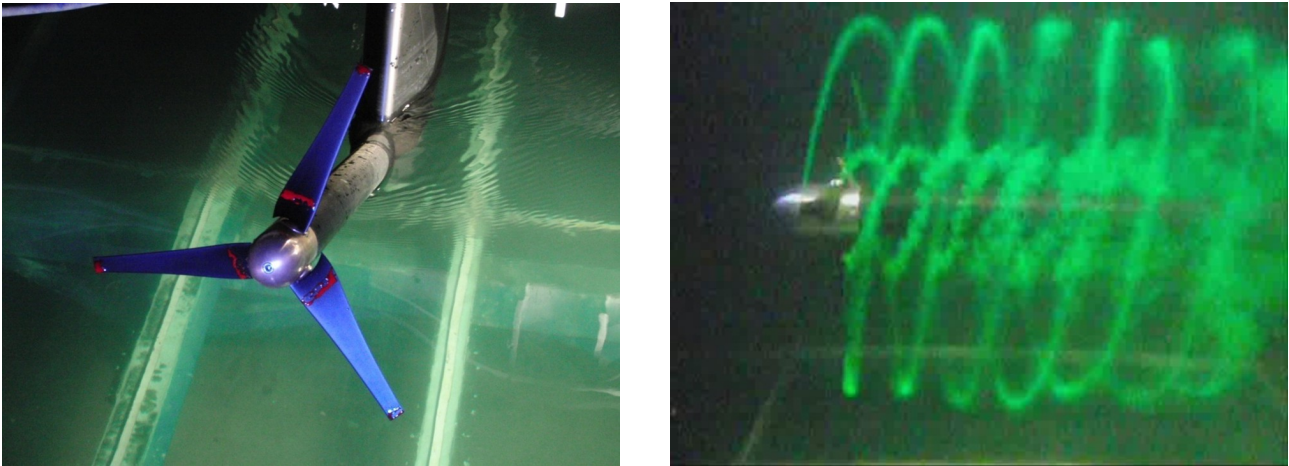


Figure 2: Image of the rotor with dye (left) and visualization of tip and root vortices (right)

Most of the plot in figure 3a show the wake region while the upper-left corner shows the flow outside the wake. In the border between these two regions, the tip vortices are seen along a line from $(z/D, y/D) = (0.0, 0.5)$ to $(z/D, y/D) = (0.4, 0.6)$. The tip vortices are seen as local “turning” of the in-plane velocity vectors, but they also leave local traces in the out-of-plane velocity component since the vortices have an angle with measurement plane. The flow outside the tip vortices have no flow in the x -direction, while clear patterns of flow in the positive x -direction is seen in the wake. This is particular strong near the hub, where the root vortices are found, but further way from the hub, traces of rotor blade passages are seen. These traces are vertical for the design tip speed ratio $\lambda = 5$, while other angles are seen for other values of λ .

One of the snapshots is shown in figure 3b. The flow has the same main features as the mean field, but the tip vortices are much more local. Some variation in the tip vortex positions are observed when several snapshots are examined. The flow in the wake contains small scale variations that both reflects turbulence and measurement noise.

To identify the tip vortices, the out-of-plane component ω_x of the vorticity vector is shown for the snapshot in figure 3c as color with in-plane velocity vectors on top. The tip vortices show clearly up as blobs of strong positive vorticity. Small blobs of strong negative or positive vorticity also shows up at location with reflections from blades, rotor hub or gearbox. These blobs are therefore located at specific regions of the flow. The vorticity field is now used to estimate the position of the tip vortices. The following procedure is used. Only points with a vorticity larger than a chosen value are considered. Here a value of $\omega_x D/U = 25$ is chosen based on visual inspection of many snapshots. Points from regions with known reflections are excluded and vortices are therefore first identified from for $z/D > 0.1$. A vortex is identified if at least three points with $\omega_x D/U > 25$ are connected. Two points are considered connected if the second point is in a 3×3 region centered around the first point. The center of the group of connected points is found as the average of point coordinates weighted with the vorticity in each point.

Figure 4 shows plots of all vortices identified. To give better coverage of the region with tip vortices, a measurement plane that has been shifted $0.2D$ in the y -direction compared to figure 3 is used. A second measurement that also has been shifted $0.8D$ in the z -direction is used to track tip vortices at more downstream positions. Figure 4 shows a plot for seven different values of λ . The dots are color-coded with rotor angle θ distributed in a rainbow like color schema with red being $\theta = 0^\circ$, orange $\theta = 15^\circ$ and so on to magenta being $\theta = 105^\circ$. The overlap between the two measurement planes is near $z/D = 0.9$ and higher intensity of points are therefore seen here. For $\lambda \geq 5$, a separate group of magenta dots (corresponding to $\theta = 15^\circ$) is seen near $(z/D, y/D) = 0.18, 0.47$). This is an artifact created from a reflection of one of the rotor blades in the background of the images. Looking first at the plot for $\lambda = 5$, the dots are organized in a narrow band for $z/D < 0.8$. The color changes smoothly and systematically moving downstream in the band. This shows that the tip vortices are distanced in a regular pattern and that they moves smoothly downstream with increasing angle. There is some spread of the single position of the same color. This probably reflects both variations in vortex shape (vorticity distribution) and the vortex position. At $z/D = 0.6$ there is a slight change of direction of the band of vortices. This occurs near the fourth group of red dots indicating four blade passages. Shortly after the width of band increases gradually and colors also tend to get more mixed.

For increasing λ the distance between groups of dots with the same color decreases indicating a shorter distance between tip vortices. This is consistent with the higher speed of the rotor. The slight change of direction of the band of vortices occurs consistently near the fourth group of red dots, which gets closer to the rotor with increasing λ . Further downstream the dots are organized in larger clusters with a much larger diameter than the width of the band of vortices near the rotor. The diameter for the first group is about $0.2D$ and increase for downstream groups.

The plot $\lambda = 4$ follows a somewhat similar pattern, but does not show the slight change in direction of the band. However, a change of the width of band of vortices also changes near the fourth group of red dots. In general, the vortices are organized in a broader band that for the higher values of λ The vortices seems to get fewer further downstream. For $\lambda = 3$ this is more pronounced and the vortices seems slowly disappear for $z/D > 0.4$.

The observations can be interpreted as follows: for $\lambda \geq 5$, the vortices are moving regularly until four blade passages have passed. Then an instability occurs and this probably develops into vortex pairing. For higher values of λ (e.g. $\lambda = 7$) three vortices seems to

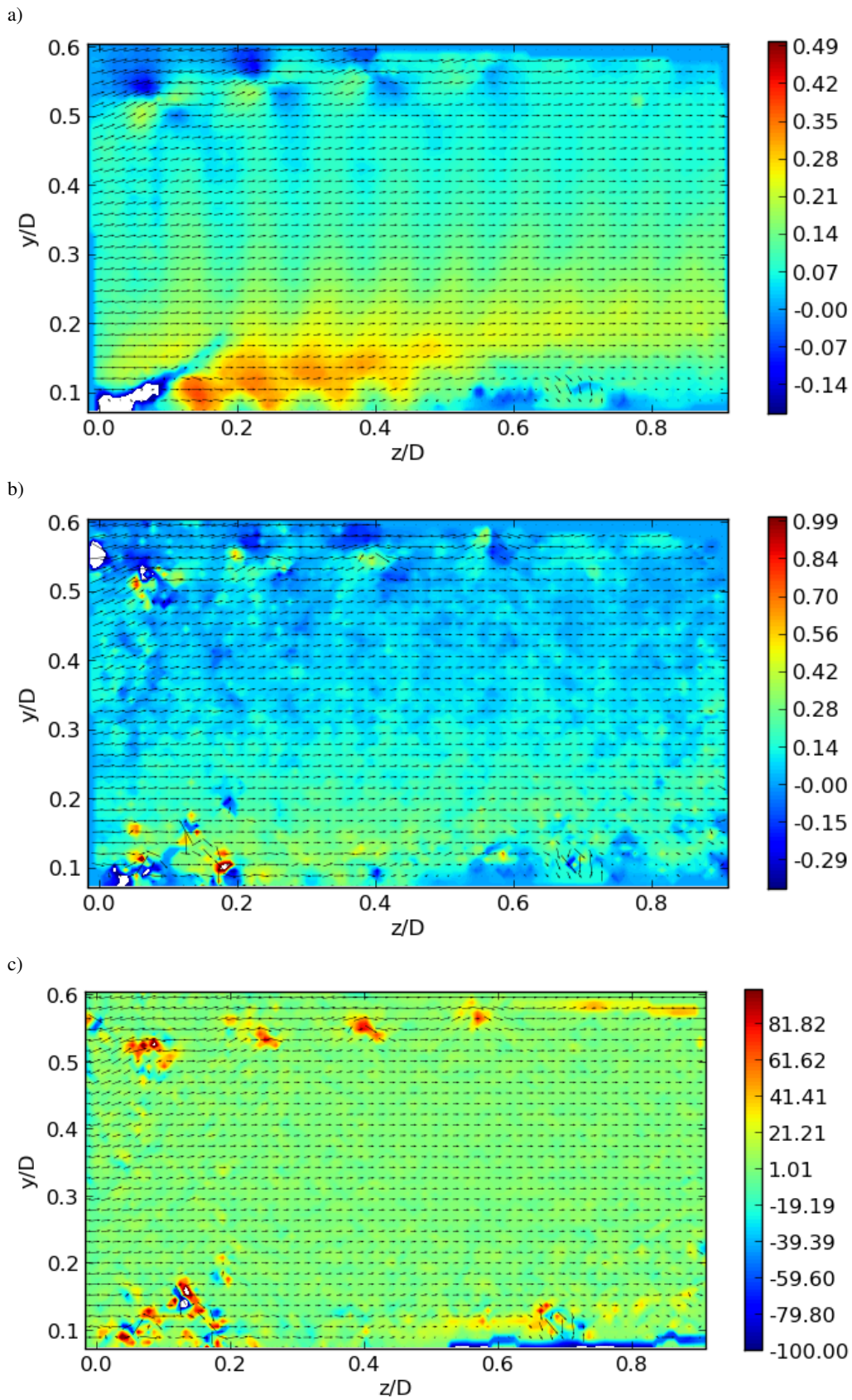


Figure 3: Measurements in the near-wake of the rotor for $\lambda = 5$ and rotor angle $\theta = 45^\circ$: a) mean field, b) snapshot and c) out-of-plane vorticity field for the snapshot. For a) and b), color shows out-of-plane velocity component u/U and for c) color shows dimensionless vorticity $\omega_x D/U$. Only every second in-plane vector is shown in each direction.

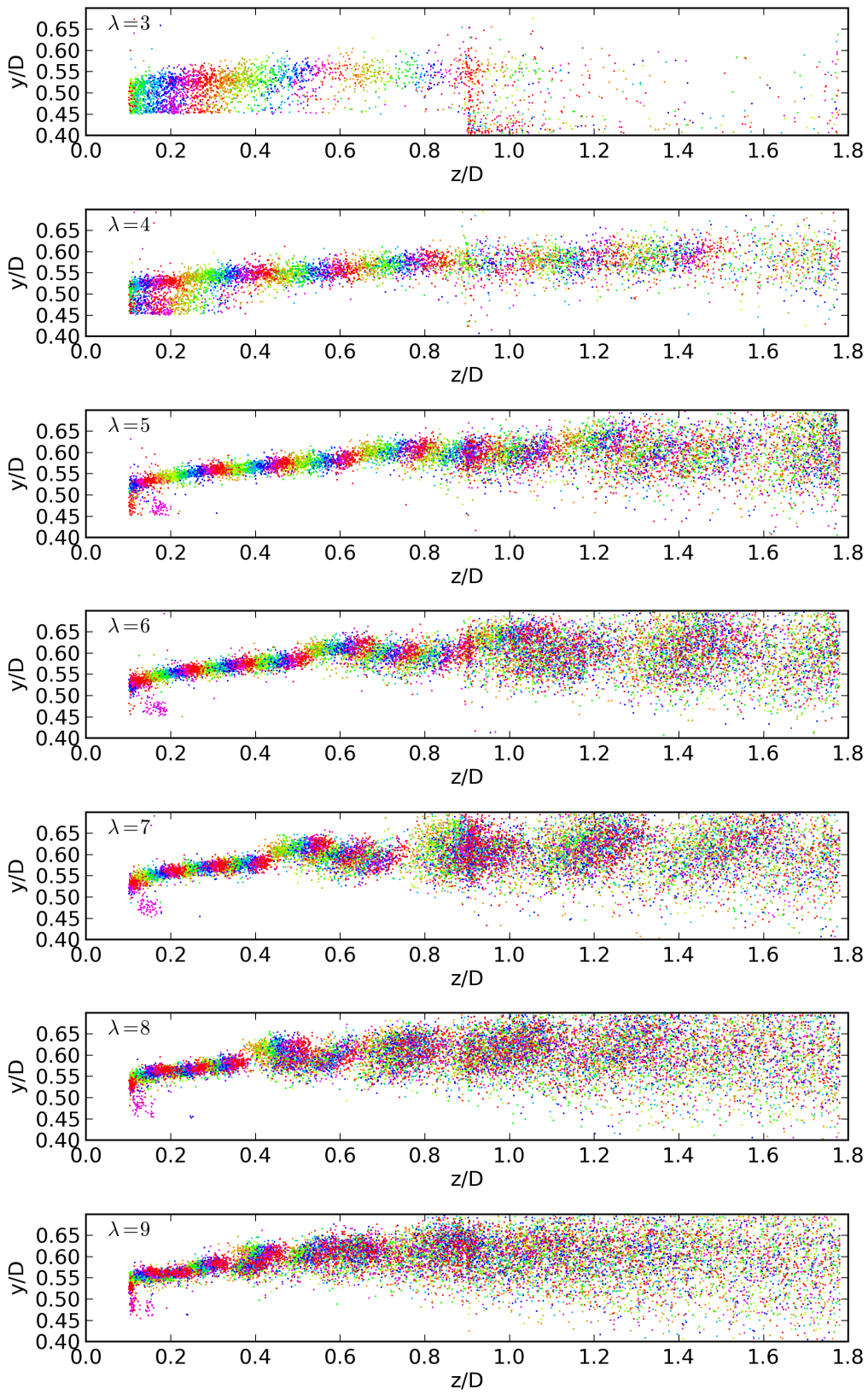


Figure 4: Positions of instantaneous vortex centers for different tip speed ratio λ (value of λ in upper left corner of each plot). Color indicate different rotor angle positions θ .

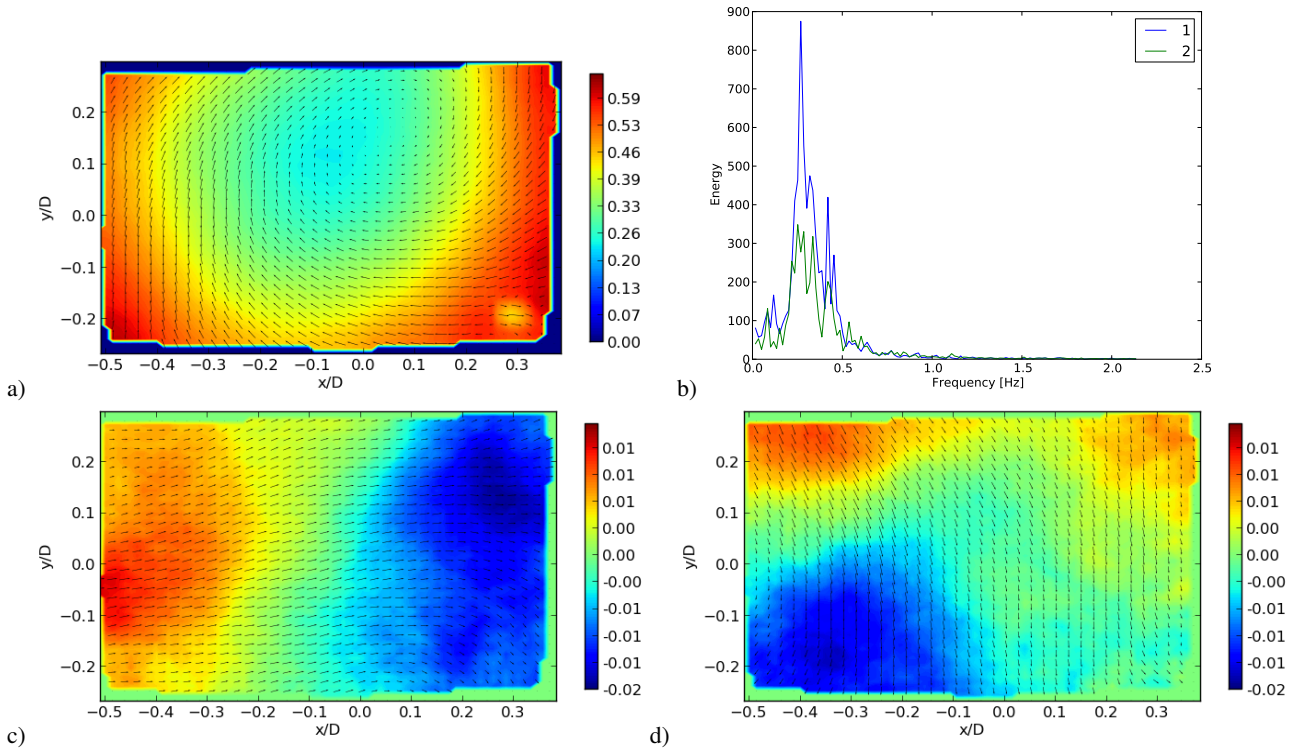


Figure 5: Measurement at the $z/D = 4$ plane for $\lambda = 5$: a) mean field, b) frequency spectra for the reconstruction coefficients of the two first POD modes, c) first POD mode, d) second POD mode. Color in plots show the out-of-plane component. Only every second in-plane vector is shown in each direction.

form a new larger vortex, since the same color is seen at three different positions when a new group is being formed. The result is fewer vortices that are more irregular in position. This is also evident in phase-averaged plots (not shown). For $\lambda < 5$, the instability is less pronounced and instead the vortices seem to decay and slowly disappear. However, this could partly be caused by the fact that lower levels of vorticity in the tip vortices for lower values of λ , makes the vortices less detectable by the procedure for finding vortex positions. The broader bands of the vortices close to the rotor is probably also caused by stall occurring at the rotor blades for low values of λ .

5. Downstream wake flow

To investigate the flow further downstream of the rotor, planes perpendicular to main flow direction z are used. This is achieved by rotating the laser sheet around the axis of the laser beam. The free stream velocity is $U = 0.45$ m/s. Camera positions are not changed, but the Scheimpflug mounts are adjusted to the new plane. The images has been processed with Dantec DynamicStudio version 3.4 using 32×32 pixel interrogation windows. By traversing the rotor, several positions from $z/D = 1.5$ to $z/D = 5$ are investigated. In each position at least 400 snapshots are taken at 4.3 Hz, which is the maximum recording speed of the PIV system. The recordings are not synchronized with rotor position.

An example of a measurement plane is shown in figure 5. This is at the plane at $z/D = 4$ for $\lambda = 5$ and it shows typical results. The mean field in figure 5a shows a near axi-symmetric region with low values of w in the core of the wake. A narrow band near the borders of the plot have exactly zero velocity and this denotes regions with no data due to no overlap between the images from the two cameras. There is a slight asymmetry that is believed to be caused by the presence of the “tower”, i.e., the cylinders holding the gearbox. There is some uncertainty on the exact position of the origin of the coordinate system. Further data processing is expected to give a more precise position. The in-plane vectors show a clear rotation around the region with low w . The measurements clearly does not cover the full wake cross section and therefore the free stream velocity is never reached.

To analyze the dynamics of the wake, Proper Orthogonal Decomposition (POD) is applied on each series of snapshots using the same methodology of snapshot POD used in [8]. In this method the first POD modes represent the statistical most energetic variations from mean field. The first and second POD modes are shown as figure 5c and 5d. The first POD modes show strong variation in the out-of-plane direction: positive variation for negative values of x and negative variation for positive values of x . When added to the mean field, the effect is to displace the low velocity core in the wake in horizontal direction. The second mode is somewhat similar to the first mode with strong variation in the positive and negative out-of-plane direction for positive y and negative y , respectively. The pattern is less uniform, probably because the measurement section covers less of the wake in the y -direction. When added to the mean field, the main effect of POD mode 2 is the displace the low velocity region in vertical direction.

The first POD modes can often be used to reconstruct large scale flow dynamics of snapshots. For a given snapshot, a reconstruction

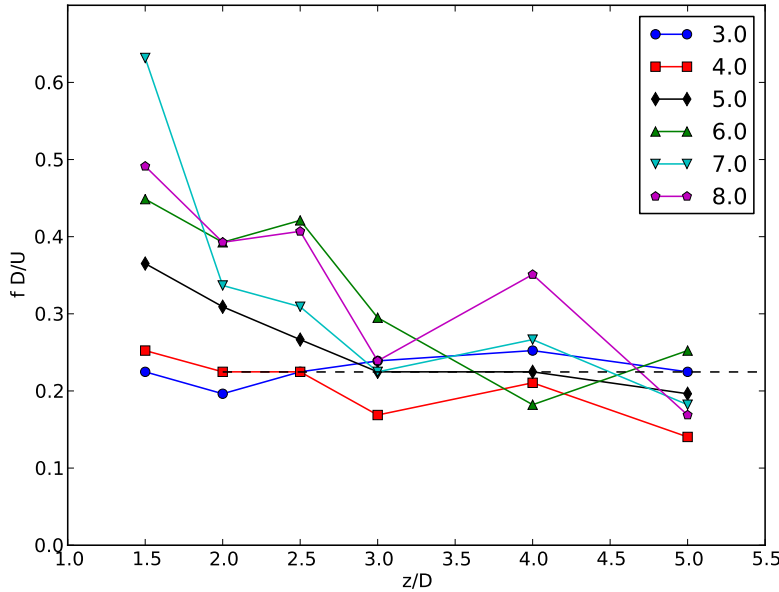


Figure 6: Dominating frequency for the first POD mode for different positions z/D and tip-speed-ratio λ (shown in legend).

coefficients for each POD modes can be found by projecting the snapshot (after the mean field has been subtracted) onto the POD mode. The reconstruction is then found by multiplying each POD mode with its reconstruction coefficient, summing and then adding the sum to the mean field. The reconstruction coefficient for the first two POD modes found for a time series of snapshots therefore represent some of the large scale variation in that time series. Inspection of the times series show that the reconstruction coefficients for the two POD modes have a variation similar to a cosine and sine variation, overlaid with some noise. This suggests systematical movement of the wake core in a circular pattern around the z -axis. The frequency of this motion can be investigated by calculating the frequency spectrum for each reconstruction coefficient. This is shown in figure 5b. The first modes reconstruction coefficient has a clear peak at $fD/U = 0.22$. The second mode's reconstruction coefficient has a less clear peak close to this frequency.

The POD analysis and determination of peak in spectrum for the first modes reconstruction coefficient is made for all combination of positions z and tip speed ratios λ . The result is shown in figure 6. For positions $z/D \geq 3$ the frequency is in almost all cases close the $fD/U = 0.2$. Mean mean value of all frequencies for $z/D \geq 3$ is $fD/U = 0.22$ and this value is shown as a dashed line in figure 6. For cases with $\lambda < 5$, the frequency also agrees well with this mean value. For $\lambda \geq 5$, the frequency increases with decreasing z . Inspection of the spectra shows much broader distributions of frequencies and less pronounced peaks.

The POD analysis is not done under optimal conditions. The measurements plane does not cover a full cross section of the wake. This means that the full dynamics of the wakes is not captured. The number of samples (~ 400) are relatively small both for the convergence of the POD modes, especially because the POD modes are not uncorrelated. Also, the number of samples are relatively low for analysis of frequencies. The present analysis should therefore be considered as a preliminary study of the wake dynamics. However, the results consistently indicate that the wake a few diameters downstream of the rotor has systematic precessing of the wake core and that frequency of the this precessing is about $fD/U = 0.22$ and is independent of the rotor speed.

6. Discussion and conclusions

Measurements with stereoscopic PIV is demonstrated to be a useful way to investigate the flow in the wake of a model wind turbine. Reports of similar measurements, e.g. [4], have used two-component PIV. This captures tip vortices well, but adding the third velocity component, reveal details on the rotating flow inside the wake. The effect of the root vortices is clearly seen and also, the rotor blades leave traces with high velocity in the direction of rotation.

The tip vortices can clearly be identified using the local out-of-plane component of the vorticity vector. For low tip speed ratio λ the vortices are less strong and decays while moving down stream. For $\lambda \geq 5$, the vortices move very regularly near the rotor, but after about 4 blade passages have occurred, an instability seems to develop. For higher values of λ this results in new larger vortices created my merging of three tip vortices.

Further downstream analysis with POD of PIV measurements in cross plane of the wake, suggest that systematically precessing of the vortex core occurs and that the frequency of this precessing is $fD/U = 0.22$. This frequency seems to be independent of the rotor speed. The frequency is similar to the dominating frequency observed behind sphere, where Achenbach [9] finds values the Strouhal number fD/U to be slightly less than 0.2. Achenbach also finds that a vortex separation point rotates around the sphere. There may therefore be some similarities between the two types of flow.

The present measurements in the cross plane are not optimal and should be improved by covering more of the wake cross section and use more data samples to give a stronger statistical significance. In present measurements, the gearbox is larger than the rotor hub. The gearbox could therefore itself act as sphere-like object that influences the wake flow. A new experiments would therefore benefit from smaller design of device holding the rotor axis.

REFERENCES

- [1] Gunnar C. Larsen *et al.* TOPFARM - next generation design tool for optimisation of wind farm topology and operation. Technical report, Risø National Laboratory for Sustainable Energy Technical University of Denmark, 2011. Risø-R-1805(EN).
- [2] J. Whale, K. H. Papadopoulos, C. G. Anderson, C. G. Helmmis, and D. J. Skyner. A study of the near wake structure of a wind turbine comparing measurements from laboratory and full-scale experiments. *Solar Energy*, 56(6):621–633, 1996.
- [3] J. G. Schepers and H. Snel. Model experiments in controlled conditions. Technical report, Energy research center of the Netherlands, 2007. ECN-E-07-042.
- [4] Michael Sherry, John Sheridan, and David Lo Jacono. Characterisation of a horizontal axis wind turbine’s tip and root vortices. *Experiments in Fluids*, 54:1417, 2013.
- [5] Wei Zhang, Corey D. Markfort, and Fernando Porté-Agel. Near-wake flow structure downwind of a wind turbine in a turbulent boundary layer. *Experiments in Fluids*, 52:1219–1235, 2012.
- [6] M. S. Selig, J. J. Guglielmo, A. P. Broeren, and P. Giguere. Summary of low-speed airfoil data. In *SolarTech Publication*, volume 1, page 292, Virginia Beach, Virginia, 1995. SolarTech Publication.
- [7] H. Glauert. *Airplane propellers Aerodynamic Theory*. Springer, 1935. pp. 169-360.
- [8] Knud Erik Meyer, Jakob M. Pedersen, and Oktay Özcan. A turbulent jet in crossflow analysed with proper orthogonal decomposition. *Journal of Fluid Mechanics*, 583:199–227, 2007.
- [9] Elmar Achenbach. Vortex shedding from spheres. *Journal of Fluid Mechanics*, 62(2):209–221, 1974.